



Hysteretic behavior of high-strength bar reinforced concrete columns under cyclic loading

Xiangyong Ni^{1,2} · Yizhu Li² · Yonghui Hou³

Received: 24 July 2022 / Accepted: 25 December 2022 / Published online: 3 January 2023
© The Author(s), under exclusive licence to Springer Nature B.V. 2023

Abstract

Hot-rolled ribbed bar (HRB) 600 is a new type of high-strength (HS) reinforcement. Its tensile stress–strain curves show an obvious yield plateau, which can be used to effectively improve the seismic performance and reduce the reinforcement ratios for concrete members. To better understand the effect of HRB600 reinforcement on the hysteretic behavior of concrete columns, cyclic tests are first conducted. Subsequently, a hysteretic model for such columns is proposed. The modeling method is established by combining the skeleton curve and hysteretic rule. The skeleton curve is simplified as a trilinear model represented by yield, peak and ultimate points, and the hysteretic rule is established based on the experimental hysteretic curves obtained in this paper. Meanwhile, numerical models are established by OpenSees to simulate the hysteretic behavior of HS bar reinforced concrete columns. Finally, the accuracy of the proposed model and numerical models are compared, then evaluated based on experimental data. The research results show that the proposed model and numerical models show a similar prediction accuracy and can be used to well predict the hysteretic behavior of concrete columns built with HRB600 steel bars. The Bernoulli–Euler assumption and plastic hinge theory can be extended for estimating the strength and deformation of HRB600 steel bar reinforced columns.

Keywords Concrete columns · HRB600 steel bars · hysteretic model · Skeleton curvature · Hysteretic rule

1 Introduction

A reinforcement with a yield strength of 500 MPa or greater is defined as high-strength (HS) reinforcement (NEHRP 2014). High-strength steel bars can be used to reduce the reinforcement ratios for concrete structures, reduce the processing and transportation costs

✉ Xiangyong Ni
20310091@tongji.edu.cn

¹ State Key Laboratory of Disaster Reduction in Civil Engineering, Tongji University, Shanghai, China

² Key Laboratory of Concrete and Prestressed Concrete Structures of Ministry of Education, Southeast University, Nanjing, China

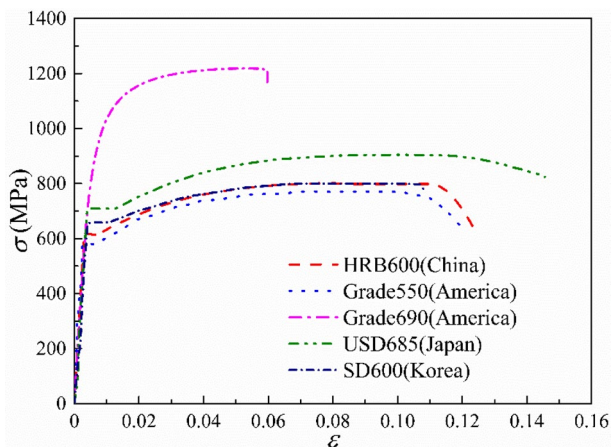
³ China Construction Second Engineering Bureau Ltd., Shanghai 200135, China

of steel bars, and improve the mechanical performance of reinforced concrete members. Meanwhile, high-strength steel bars can solve the problem of steel bar congestion in construction to improve the construction quality. Therefore, the application of high-strength reinforcement in concrete structures is beneficial for energy savings and emission reduction and has good economic, environmental and social benefits. Reinforced concrete columns are the main vertical bearing members of overall structures and are also used to resist horizontal loads generated by earthquakes or wind, so the safety of column members is important for such structures. HS reinforcement can take the form of longitudinal steel bars and stirrups for concrete column members. However, the permissible maximum strength grade for longitudinal reinforcement in the Chinese code is HRB500 with a nominal yield strength of 500 MPa, and HRB600 is expected to be approved in Chinese codes in the next few years. Consequently, more studies should be conducted to promote the application of HRB600 reinforcement in concrete structures.

Many types of high-strength reinforcement have been developed worldwide, including America Grade 550 MPa (80 psi) and 690 MPa (100 psi) (Li et al., 2019), Japan USD 685 MPa (Hwang et al., 2014), Korea SD600 MPa (Ousalem et al. 2009), and China HRB600 MPa. Figure 1 shows the strain–stress curves for the above types of high-strength reinforcement. High-strength reinforcing bars have a similar elasticity modulus. HRB600, SD600, and USD685 reinforcing bars show yield plateaus and considerable elongation, which are different from that for Grade 550 MPa and 690 MPa reinforcement (America). From a comparison of the strain–stress curves obtained for HRB600 and SD600 with the same nominal yield strength of 600 MPa, the SD600 reinforcement shows a longer yield plateau, larger yield strength, and similar elongation. Therefore, the mechanical properties of HRB600 reinforcement are different from that of other types of high-strength reinforcement. On the other hand, the key performance specifications of HRB600, such as yield strength, yield plateau, and ultimate strain, can meet the engineering requirements of other countries, so such reinforcement can be used for civil engineering in other countries. HRB600 is a new type of high-strength reinforcing bar developed in China, but the current design specifications do not cover such steel bars, mainly due to the lack of relevant experimental and theoretical research.

HS steel bars can be used as longitudinal bars and stirrups for concrete members, and the application of HS steel bars in columns has been experimentally investigated in

Fig. 1 Stress–strain curves for high-strength reinforcing bars



depth. Restrepo et al. (2006), Matsumoto et al. (2008), Ousalem et al. (2009), Rautenberg et al. (2011), Su et al. (2014a, b), Legage et al. (2012), Link et al. (2014), Ou et al. (2015), Sokoli et al. (2014), Ibarra et al. (2016), Trejo et al. (2016), Lim et al. (2017), Aboukifa et al. (2021), Ding et al. (2021), He et al. (2020), and Zhang et al. (2020) have conducted cyclic loading tests on column specimens with high-strength longitudinal bars. The test results show that compared with normal strength bar reinforced concrete columns, HS longitudinal bar reinforced concrete columns show similar ductility and reduced energy dissipation capacity, which indicates that HS longitudinal reinforcement can solve the problem of reinforcement congestion and save reinforcement ratios without affecting the seismic performance of the columns. The test results also found that the bond-slip failure phenomenon occurs between HS longitudinal steel bars and normal strength concrete, while the bond-slip failure phenomenon does not occur between HS longitudinal steel bars and ultra high-performance fiber concrete. Thomsen et al. (1994), Xiao-Martirosyan et al. (1998), Paultre et al. (2001), Shi et al. (2011), and Hwang et al. (2005) have experimentally investigated the influence of HS stirrups on the seismic performance of columns. The test results indicate that HS stirrups can develop a strong confinement on the concrete columns under high axial compression. HS stirrups can save reinforcement ratios without reducing the seismic performance of the columns and can help the columns obtain satisfactory ductility. HS stirrups have little effect on the strength of the columns under small axial loading ratios, while they can significantly increase the strength of the columns with high axial compression ratios. The above studies also find that HS stirrups can be used to significantly improve the postpeak deformation and ductility of columns. For the failure of column specimens in shear, high-strength stirrups cannot significantly improve the shear strength of column specimens, and HS stirrups generally stay in an elastic state, but the deformation and energy dissipation capacity of the column specimens can be increased with such reinforcement.

The above experimental studies have demonstrated that the application of high-strength steel bars in concrete columns has high feasibility and can be used to effectively reduce the reinforcement ratios in concrete columns. Then solve the problem of reinforcement congestion. To promote the application of HS steel bars in concrete columns, more theoretical research is needed, but related studies are limited at present (Ni et al. 2019). The flexure strength of normal strength bar reinforced concrete columns can be accurately predicted using the theory of the Bernoulli–Euler assumption, but for high-strength steel bars, the stress–strain characteristics are quite different from those of normal strength steel bars, especially large yield strain, so it is necessary to study the applicability of the Bernoulli–Euler assumption to high-strength bar reinforced concrete columns. The nonlinear deformation of columns under cyclic loading is commonly calculated by plastic hinge theory (Thomsen et al. 2004), and the adaptability of this theory to high-strength reinforced concrete columns needs to be investigated. The above experimental studies have found that bond-slip failure can occur between a HS longitudinal bar and concrete and can lead to an increase in the lateral deformation of the column, so the deformation caused by bond-slip cannot be ignored. Bond-slip deformation is, currently, a difficult research point. Many studies have been conducted on the hysteretic models of concrete columns built with normal strength reinforcement, but due to the application of high-strength steel bars in columns, the hysteretic characteristics of such columns are quite different from those of normal strength bar reinforced concrete columns, especially in terms of unloading stiffness and pinch effect. In conclusion, the deficiencies of the present study can be summarized as follows:

- (1) The mechanical property of HRB600 reinforcement newly developed in China show some differences in material properties compared with existing high-strength steel bars, while previous research into HS steel bars in concrete structures has mainly focused on a yield strength of 500 MPa and below or 900 MPa and above, and the experimental research into the application of HRB600 reinforcement in columns remains limited.
- (2) The hysteretic behavior of HS bar reinforced concrete columns has been experimentally investigated in depth, but few theoretical studies have been conducted. A hysteretic model can be used to predict the hysteretic response of the columns under cyclic loading, which can also be used for the nonlinear analysis of the column members in the whole structure. The hysteretic performance of concrete columns built with HS reinforcement is different than that of columns with normal strength reinforcement. However, studies based on hysteretic models of concrete columns built with HS reinforcement are scarce.
- (3) Owing to the application of HS reinforcement in concrete columns, the applicability of the Bernoulli–Euler assumption and plastic hinge theory for such columns needs to be investigated. The bond-slip between HS longitudinal bars and concrete is complex, and the deformation caused by bond-slip should be considered and mathematized. However, few related studies have been conducted.

To address the above research gaps, a cyclic loading test is first carried out for column specimens built with HRB600 reinforcement to examine the influence of stirrup spacing and axial compression ratio on the hysteretic performance. Then, a simplified calculation method for hysteretic curves is proposed by combining the skeleton curve and hysteretic rule. Finally, the proposed model is used to predict the hysteretic curves for the column specimens, and the prediction accuracy is evaluated based on the test data.

2 Test program

2.1 Column specimens

Figure 2 depicts the geometric dimensions and reinforcing arrangement of the specimens. To research the effect of stirrup spacing and axial compression ratio on hysteretic behavior, four RC cantilever column specimens were tested under cyclic loading. The specimens' precise design specifications can be obtained in a prior study (Li et al. 2018). The longitudinal bars of the column specimens adopted HRB600 reinforcement with a diameter of 16 mm ($f_y=615$ MPa) and HRB400 reinforcement with a diameter of 16 mm ($f_y=471$ MPa). Every specimen was given a unique name that could be used to identify the study parameters. The nomenclature is described as follows: the first two numerals denote longitudinal and stirrup reinforcing types, respectively, H signifies HRB600 reinforcement, and N signifies HRB400 reinforcement. The second numeral denotes the axial compression ratios for the specimens: 0.2, 0.4, and 0.5, and the axial compression ratios can be obtained by Eq. (1). The concrete utilized for the sample had a C50 strength rating (the measured value is 47.4 MPa). The column's longitudinal bars comprised 12 steel bars with a diameter of 16 mm, with a longitudinal bar ratio of 1.97 percent. The stirrup was constructed of an HRB400/600 steel bar with a diameter of 8 mm and yield strengths of 437 MPa and 629 MPa, respectively, and a well-shaped compound stirrup form. Stirrup spacings of 70 mm and 105 mm stirrup spacing were available,

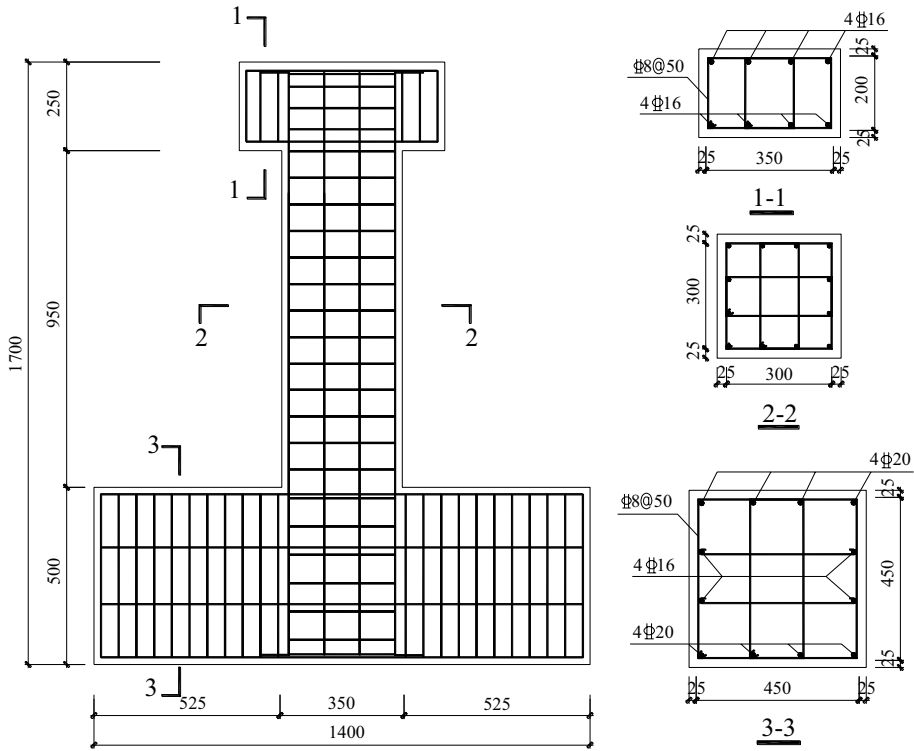


Fig. 2 Dimensions and reinforcement

with volume stirrup ratios of 1.91% and 1.28%, respectively. Table 1 lists the details for the above six specimens.

$$n = \frac{N}{f_c A} \tag{1}$$

Table 1 Design parameters

Specimens	Axial load ratio n	Longitudinal reinforcement			Stirrup reinforcement		
		Strength grade	d_l /mm	ρ /%	Strength grade	d_t /mm	s /mm
NN-0.2-1	0.2	HRB400	16	1.97	HRB400	8	70
NH-0.2-2	0.2	HRB400	16	1.97	HRB600	8	70
HH-0.2-3	0.2	HRB600	16	1.97	HRB600	8	105
HH-0.2-4	0.2	HRB600	16	1.97	HRB600	8	70
HH-0.4-5	0.4	HRB600	16	1.97	HRB600	8	70
HH-0.5-6	0.5	HRB600	16	1.97	HRB600	8	70

Note: d_l is the diameter of the longitudinal reinforcement; ρ is the ratio of the longitudinal reinforcement; d_t is the diameter of the stirrup; and s is the stirrup spacing

where N is the axial load applied on the wall, f_c is the strength of the concrete on the test day, and A is the wall cross-sectional area.

2.2 Hysteretic response

The hysteresis responses of the specimen are generally in the shape of a plump shuttle, indicating that the specimen has good seismic performance (Fig. 3). During the initial stage, the hysteresis loop areas are very small. With increasing loading displacement, the surrounding area of the hysteretic loops continuously increases, and an obvious residual deformation occurs after unloading; when the specimen reaches the peak force, the deformation accelerates. Under the same displacement, the peak load and the slope of the curve decrease with increasing cycle number, which indicates that the specimen shows strength attenuation and stiffness attenuation under cyclic loading. Due to failure of the bond between the HRB600 reinforcement and concrete, the plumpness of the hysteresis curves becomes significantly worse, and the curve develops into an inverse S-shape in the later stage, indicating that the configuration of the HRB600 longitudinal reinforcement can reduce the hysteretic performance of the specimen in the later stage.

Table 2 summarizes the detailed experimental results obtained for the hysteretic curves of the above column specimens. Compared to Specimen NN-0.2–1 built with HRB400, the specimens built with HRB600 longitudinal reinforcement have a larger yield displacement owing to the larger yield strain of HRB600 reinforcement. Compared to Specimen NN-0.2–1 with a HRB400 stirrup, Specimen NH-0.2–1 with a HRB600 stirrup (stirrup strength is increased by 43.9%) shows a larger lateral strength ($\uparrow 15\%$) and drift ratio capacity ($\uparrow 12\%$) but smaller ductility ratio ($\downarrow 8.28\%$). Compared to Specimen NH-0.2–2 with a HRB400 stirrup, Specimen HH-0.2–4 built using a HRB600 stirrup has a larger peak strength ($\uparrow 29.3\%$) and a similar drift ratio capacity but a reduced ductility ratio ($\downarrow 29.6\%$).

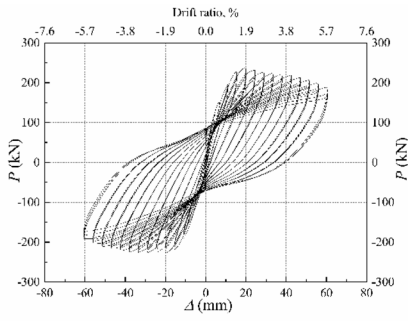
3 Simplified calculation method

3.1 Hysteretic model

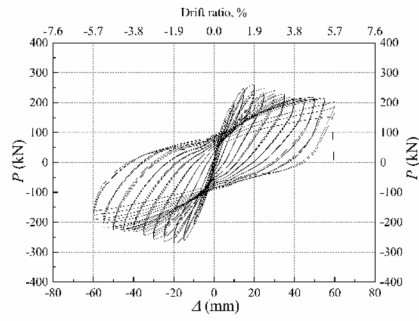
The hysteretic model for HS bar reinforced columns is composed of a skeleton curve and hysteretic rule.

3.1.1 By analyzing the above hysteretic curves, the force process for the above column specimens can be roughly divided into three stages, including the elastic stage, elastic–plastic stage from yielding to the peak point, and failure stage from Skeleton curve

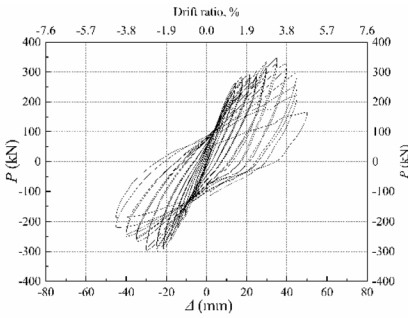
the peak point to failure, as shown in Fig. 4. Therefore, the skeleton curve is simplified into a trilinear model that can be determined using three characteristic points, namely, Y, M and U, corresponding to the yield, peak and failure points, respectively. Therefore, six parameters need to be determined to establish the skeleton curve model, which are the preyield stiffness k_1 , yield load P_y and displacement Δ_y ; stiffness k_2 , peak load P_m and displacement Δ_m ; stiffness k_3 , ultimate load P_u and displacement Δ_u . The skeleton curve can be expressed as Eq. (2).



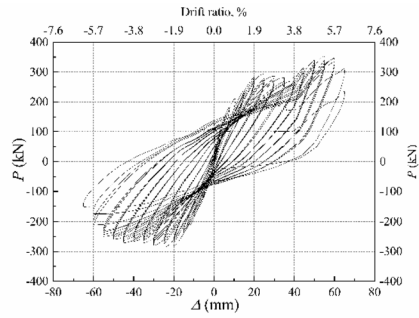
(a) NN-0.2-1



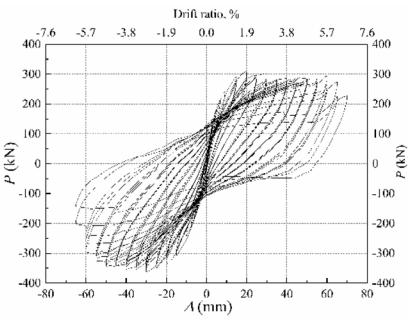
(b) NH-0.2-2



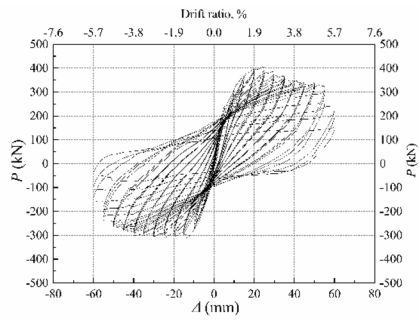
(c) HH-0.2-3



(d) HH-0.2-4



(e) HH-0.4-5



(f) HH-0.5-6

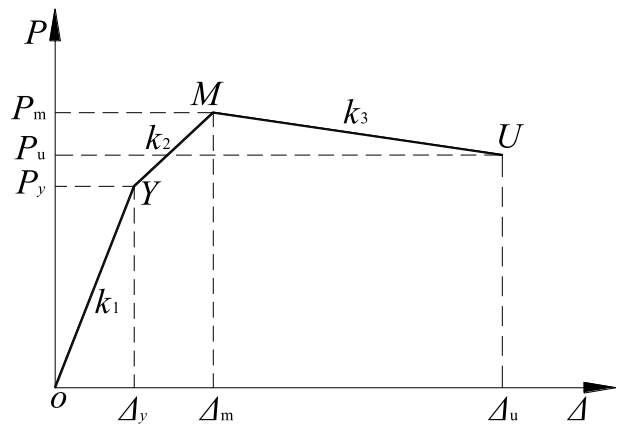
Fig. 3 Hysteretic curves

Table 2 Detailed experimental results obtained for the hysteretic curves

Specimens	Yield drift ratio δ_y (%)	Peak point		Drift ratio capacity δ_u (%)	Ductility ratio (δ_p/δ_u)
		F	δ_p (%)		
NN-0.2-1	0.61	238	1.85	5.27	8.58
NH-0.2-2	0.71	273	1.84	5.56	7.87
HH-0.2-3	0.87	348	4.18	4.81	5.56
HH-0.2-4	0.95	353	5.06	5.67	5.98
HH-0.4-5	1.15	− 363	2.75	5.77	5.00
HH-0.5-6	0.91	406	2.32	4.21	4.62

Note: the unit for F is kN

Fig. 4 Trilinear model for the skeleton curve

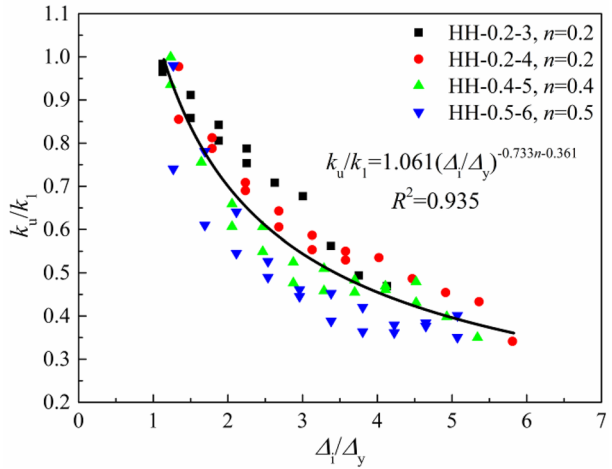


$$P = \begin{cases} \frac{P_y}{\Delta_y} \cdot \Delta & 0 \leq \Delta < \Delta_y \\ \frac{P_m - P_y}{\Delta_m - \Delta_y} \cdot (\Delta - \Delta_y) + P_y & \Delta_y \leq \Delta < \Delta_m \\ \frac{P_u - P_m}{\Delta_u - \Delta_m} \cdot (\Delta - \Delta_m) + P_m & \Delta_m \leq \Delta < \Delta_u \end{cases} \quad (2)$$

3.1.2 Hysteretic rule

With increasing loading displacement (especially after yield displacement), both the loading and unloading stiffnesses of the columns degrade. The line between the unloading point and point where the force is unloaded to 0 is the unloading line, and the slope represents the unloading stiffness k_u . k_u changes with increasing loading displacement, and the axial ratios have a significant influence on the unloading stiffness attenuation. Li et al. (2014) reported that the unloading stiffness of an HS concrete column confined by an HS stirrup is related to the volume ratio of the stirrups and axial loading ratios, and they obtained the formula for unloading stiffness by regression. Guo et al. (2004) studied the variation law for unloading stiffness of concrete columns under different axial

Fig. 5 Unloading stiffness of the columns



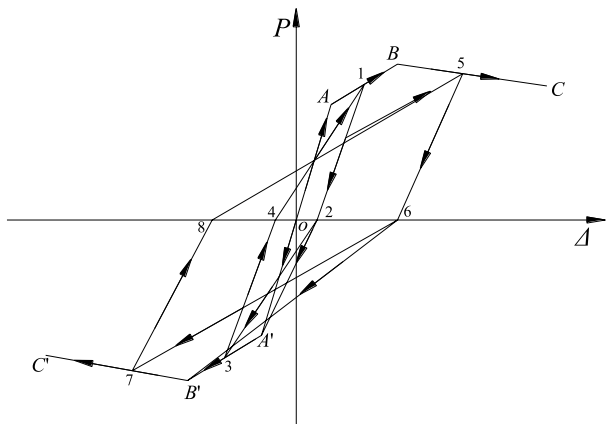
compression ratios and considered that the axial loading ratio is a critical parameter that can influence unloading stiffness. Meanwhile, a regression formula for unloading stiffness is proposed. Figure 5 presents the variation in unloading stiffness attenuation rates (k_u/k_1) with ductility ratios for the above column specimens. The unloading stiffness formula can be obtained from regression analysis and is expressed as Eq. (3):

$$k_u = 1.061k_1 \left(\frac{\Delta_i}{\Delta_y} \right)^{-0.733n-0.361} \tag{3}$$

where k_1 is the equivalent elastic stiffness, $k_1 = P_y/\Delta_y$; Δ_i is the maximum displacement experienced by the specimen before unloading; and n is the axial compression ratio.

Based on the above experimental hysteretic curves, the hysteretic rule for the hysteretic model of concrete columns can be summarized as shown in Fig. 6, and its hysteresis rules are described as follows:

Fig. 6 Hysteresis rules



- (1) Points A and A' are yield points, B and B' are peak points, and C and C' are failure points.
- (2) The load–displacement curve moves along Path O-A from the beginning to the yield point, and the loading stiffness is k_1 (the equivalent elastic stiffness before yielding). If an unloading curve is performed by following Path O-A, the unloading path returns along the original loading path. When unloading to the origin, reverse loading is carried out along Path O-A'.
- (3) After yielding, the loading stiffness changes to k_2 , and the loading path goes along Path A-B. At this point, if the unloading is carried out in Section A-B, the unloading path is carried out along Line 1–2, and the unloading stiffness k_u can be calculated according to Eq. (3). After unloading to Point 2, if the specimen fails to yield in the reverse direction, the path points to the reverse yield Point A', that is, reverse loading is carried out along Path 2-A'-B'; if the specimen has yielded in the reverse direction, the maximum point pointing principle is adopted to point to the maximum displacement (Point 3) experienced in the previous loading, that is, reverse loading is carried out along Path 2–3-B'. When reverse unloading is carried out in Section A'-B', unloading is carried out along Path 3–4, and the unloading stiffness k_u can be calculated according to Eq. (3). For the case of reverse unloading to 0 followed by forward loading, the loading path points to the maximum displacement (Point 1) experienced at the previous loading, that is, along Path 4–1-B.
- (4) After the specimen reaches peak point B (B'), the loading stiffness changes to k_3 , and the loading path proceeds along Path B-C. At this point, if the unloading is carried out in Section B-C, the unloading path is carried out along Path 5–6, and the unloading stiffness k_u is calculated according to Eq. (3). If the reverse load does not reach the peak load point (point B'), the path points to the reverse peak point B', that is, along Path 6-B'-C'. If the reverse load reaches the peak load, the loading path points to the maximum displacement (Point 7) in the previous loading, that is, to proceed along Path 6–7-C'. For the case of reverse unloading in Section B'-C', unloading is carried out along Paths 7–8, and the unloading stiffness is calculated according to Eq. (3). For reverse unloading to 0 (Point 8) and forward loading, the loading path follows Path 8–5. Other loading and unloading paths are the same as that for the preceding rules.

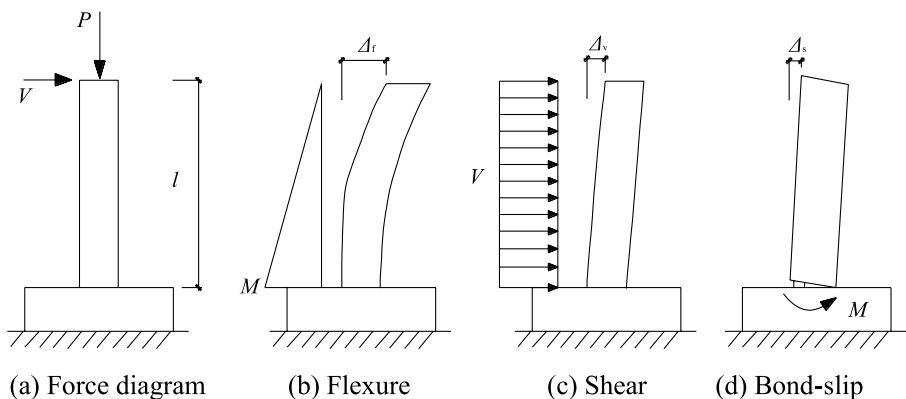


Fig. 7 Lateral deformation

3.2 Lateral deformation

The lateral displacement is composed of three parts: flexure deformation (Δ_f), shear deformation (Δ_v) and deformation (Δ_s) caused by the bond-slip, as shown in Fig. 7. Before yielding, the curvature formed by the bending moment and the shear deformation is linearly distributed along the column height. After yielding, a plastic hinge forms at the column bottom. The curvature formed by the bending moment in the plastic hinge region is obviously larger than that of the elastic segment. The shear displacement of the column is composed of shear deformation in the plastic hinge zone and elastic zone. The deformation caused by the bond-slip is generally small before the specimen yields. After the specimen yields, bond slip causes the column to rotate around the bottom of the column. Therefore, the lateral displacement can be expressed as follows (Wang et al. 2019a):

$$\Delta = \Delta_f + \Delta_v + \Delta_s \tag{4}$$

3.3 Yield point

3.3.1 Yield force

For the flexural-dominated member, it is generally assumed that the yield load (P_y) and displacement (Δ_y) are the load and displacement when the outermost longitudinal bars yield in the tensile direction. The stress–strain formula for compressive concrete is expressed as follows (GB 50,010–2010 2011):

$$\sigma = \begin{cases} f_c \left(1 - \left(1 - \frac{\epsilon}{\epsilon_0} \right)^2 \right) & \epsilon \leq \epsilon_0 \\ f_c & \epsilon_0 < \epsilon \leq \epsilon_{cu} \end{cases} \tag{5}$$

where f_c is the axial compressive strength of concrete; ϵ_0 is the peak strain, generally, ϵ_0 is taken to be equal to 0.002; and ϵ_{cu} is the ultimate compressive strain, generally, ϵ_{cu} is taken to be equal to 0.0033 (GB 50,010–2010 2011).

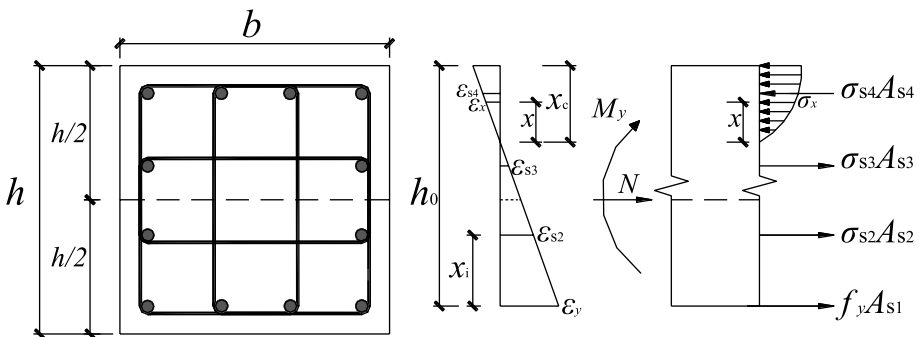


Fig. 8 Force state of the critical cross-section at the yield point of the columns

According to the assumption of a flat section, the force state of the critical cross-section at the point of yielding is shown in Fig. 8. According to the balance condition of the force, the following formulas can be obtained:

$$\sum \sigma_{si}A_{si} + N = \int_0^{x_c} \sigma_x b dx \tag{6}$$

$$M_y + \sum \sigma_{si}A_{si}x_i + N\left(h_0 - \frac{h}{2}\right) = \int_0^{x_c} \sigma_x (h_0 - x_c + x) b dx \tag{7}$$

With

$$\sigma_{si} = E_s \varepsilon_{si} = E_s (h_0 - x_c - x_i) \frac{\varepsilon_y}{h_0 - x_c} \leq f_y \tag{8}$$

$$\varepsilon_x = x \frac{\varepsilon_y}{h_0 - x_c} \tag{9}$$

where b is the width of the cross-section and h and h_0 are the height and effective height of the cross-section, respectively, where E_s is the elastic modulus of the longitudinal reinforcement, N is the axial load, M_y is the yielding bending moment of the critical cross-section when the specimen yields, x_c is the height of the concrete compression zone, f_y is the tensile yield strength of the longitudinal reinforcement, and ε_y is the tensile yield strain of the outermost longitudinal reinforcement. σ_{si} and ε_{si} are the stress and strain for the i th longitudinal reinforcing bar (positive in tension and negative in compression), respectively. x_i is the distance from the i th longitudinal reinforcing bar to the outermost tensile longitudinal reinforcing bar; x is the distance for any position along the neutral axis; and σ_x and ε_x are

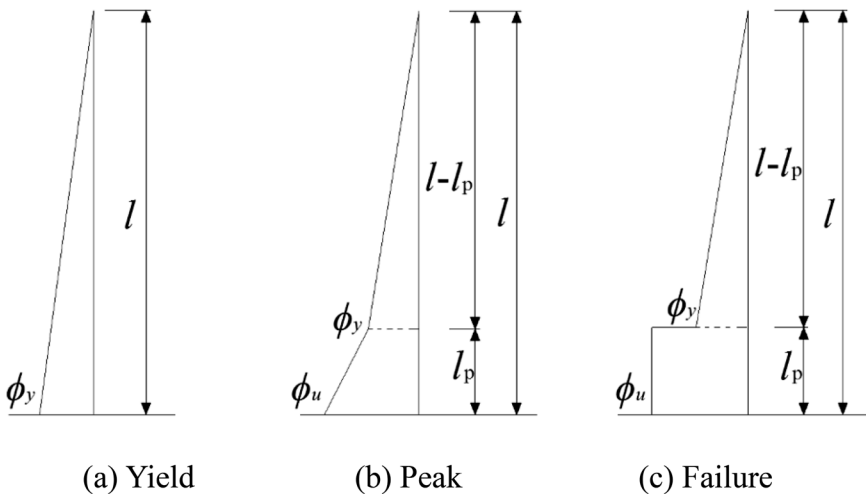


Fig. 9 Curvature distribution

the compressive stress and strain of compressive concrete, respectively, at the distance of x to the neutral axis of the cross-section.

3.3.2 Yield displacement

The yield curvature of the critical section is ϕ_y , and the curvatures generated by the bending moment are linearly distributed along the column height (Fig. 9(a)).

- (1) Flexure displacement Δ_{yf} .

Based on Bernoulli’s assumption, the displacement caused by bending deformation can be obtained from

$$\Delta_{yf} = \frac{VL^3}{3E_cI} = \frac{1}{3}\phi_y l^2 \tag{10}$$

With

$$\phi_y = \frac{\epsilon_y}{h_0 - x_c} \tag{11}$$

where V is the lateral force, I is the inertia moment of the cross-section, and E_c is the elastic modulus of concrete.

- (2) Shear displacement Δ_{yv} .

The shear displacement can be obtained from

$$\Delta_{yv} = \mu \frac{Vl}{G_c A} \tag{12}$$

where G_c is the shear modulus of concrete, $E_c/G_c = 2.5$; A is the total area of the cross-section; and μ is the nonuniform coefficient of the shear stress distribution of the rectangular section, which is equal to 1.2.

- (3) Lateral displacement caused by bond-slip Δ_{ys} .

Sezen-Setzler (2008) proposed a formula for calculating the bond slip based on experimental and theoretical analysis:

$$\Delta_{ys} = \theta_s l = \frac{\epsilon_y f_y d_b l}{8\mu_e (h_0 - x_c)} \tag{13}$$

where θ_s is the rotation angle of the rigid body generated by bond-slip, d_b is the diameter of the longitudinal reinforcing bars, μ_e is the uniform elastic bond stress, and the other parameters have the same meanings as above.

3.4 Peak point

3.4.1 Peak force

The peak point of the columns corresponds to the ultimate state of the bearing capacity, which is controlled by the maximum normal stress of the critical cross-section, and when the concrete at the compression edge reaches the ultimate compressive strain, the columns enter the peak point. The stress and strain distribution of the critical cross-section at the

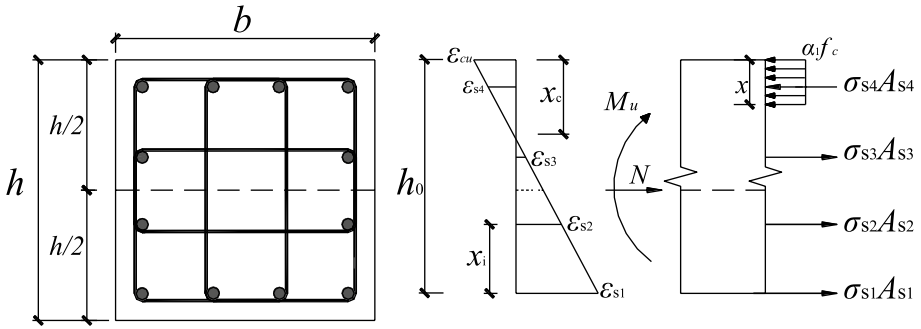


Fig. 10 Force state of the critical cross-section of the peak point

peak point is shown in Fig. 10, where the concrete at the compression edge reaches the ultimate compressive strain. From the force balance condition for the cross-section, it can be determined that

$$N = \alpha_1 f_c b x - \sum \sigma_{si} A_{si} \tag{14}$$

$$M_u = \alpha_1 f_c b x \left(h_0 - \frac{x}{2} \right) - \sum \sigma_{si} A_{si} x_i - N \left(h_0 - \frac{h}{2} \right) \tag{15}$$

where

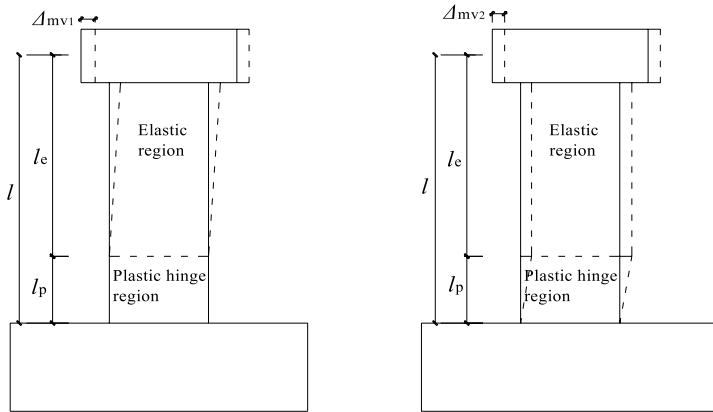
$$\sigma_{si} = E_s \varepsilon_{si} = E_s (h_0 - x_c - x_i) \frac{\varepsilon_{cu}}{x_c} \leq f_y \tag{16}$$

$$x_c = \frac{x}{\beta_1} \tag{17}$$

where α_1 and β_1 are the characteristic coefficients of the equivalent rectangular stress graph for the concrete stress distribution of the cross-section, which are adopted according to GB50010-2010 (2011), $\alpha_1 = 1.0$, and $\beta_1 = 0.8$. M_u is the maximum bending moment; x is the height of the equivalent rectangular stress diagram in the concrete compression zone; and σ_{si} and ε_{si} are the stress and strain of the i th longitudinal reinforcement (positive in tension and negative in pressure), respectively. x_i is the distance from the i th longitudinal reinforcement to the outermost tensile longitudinal reinforcement.

3.4.2 Peak displacement

At the peak point, the concrete strain at the edge of the compressive zone of the critical cross-section reaches the ultimate strain ε_{cu} , and, at this time, the curvature is the ultimate curvature ϕ_u , and a plastic hinge is formed with a height of l_p . The area outside of the plastic hinge area is still in the elastic stage. The curvature distribution for the specimen is shown in Fig. 11. The lateral displacement of the specimen is composed of the displacement generated by the upper elastic segment and that of the plastic hinge region. The displacements of the upper elastic segment and plastic hinge region are all composed of flexure, shear, and bond-slip displacements (Wang et al. 2019a), as expressed by Eq. (18):



(a) Shear deformation in the upper elastic region (b) Shear deformation in the plastic hinge region

Fig. 11 Shear displacement

$$\Delta_m = \Delta_{mf} + \Delta_{mv} + \Delta_{ms} \tag{18}$$

where Δ_{mf} , Δ_{mv} , and Δ_{ms} are the peak flexure, shear and bond-slip deformation, respectively.

(1) Flexure displacement Δ_{mf} .

The flexure displacement is composed of the displacement Δ_{mf1} of the upper elastic segment and Δ_{mf2} of the plastic hinge region, i.e., $\Delta_{mf} = \Delta_{mf1} + \Delta_{mf2}$. The displacement Δ_{mf1} can be calculated using Eqs. (10–11). The column height l in the formula should be replaced by the height l_e of the upper elastic segment. The height l_p of the plastic hinge region can be calculated according to Eq. (19):

$$l_p = 0.08l + 0.022f_y d_b \tag{19}$$

$$l_e = l - l_p \tag{20}$$

The displacement Δ_{mf2} can be obtained from

$$\Delta_{mf2} = \int_{l_e}^{l_e+l_p} x\phi(x)dx \tag{21}$$

$$\phi(x) = \frac{\phi(u) - \phi(y)}{l_p} (x - l_p) + \phi(y) \tag{22}$$

Combining Eqs. (21) and (22), the displacement Δ_{mf2} can be obtained as follows:

$$\Delta_{mf2} = \frac{1}{2}l_e l_p \phi_y + \frac{1}{2}l_e l_p \phi_u + \frac{1}{6}l_p^2 \phi_y + \frac{1}{3}l_p^2 \phi_u \tag{23}$$

With

$$\phi_u = \frac{\epsilon_{cu}}{x_c} \tag{24}$$

(2) Shear displacement Δ_{mv}

As shown in Fig. 12, the shear deformation is composed of Δ_{mv1} for the upper elastic section and Δ_{mv2} for the plastic hinge region, i.e., $\Delta_{mv} = \Delta_{mv1} + \Delta_{mv2}$. The displacement Δ_{mv1} can be calculated using Eq. (12), and the column height l given in the equation is replaced by the upper elastic section height l_e . The shear force V is replaced by the peak load. The shear displacement Δ_{mv2} can be calculated according to the shear strain ductility coefficient μ_γ proposed by Gerin-Adebar (2004). The empirical formula for μ_γ can be obtained from

$$\mu_\gamma = \frac{\gamma_u}{\gamma_y} = 4 - 12 \frac{v_y}{f_c} \tag{25}$$

It is assumed that the shear strain in the plastic hinge region is a trapezoidal distribution, in which the shear strain in the upper part of the plastic hinge region is the yield shear strain, and the shear strain at the bottom of the plastic hinge region reaches the limit shear strain. Therefore, the shear displacement Δ_{mv2} can be expressed as follows:

$$\Delta_{mv2} = \frac{1}{2}(\gamma_y + \gamma_u)l_p = \frac{1}{2}(\gamma_y + \mu_\gamma\gamma_y)l_p = \frac{1}{2}\left(5 - 12\frac{v_y}{f_c}\right)\gamma_y l_p \tag{26}$$

where

$$v_y = 0.25\sqrt{f_c} + \rho_h f_{yh} \leq 0.25f_c \tag{27}$$

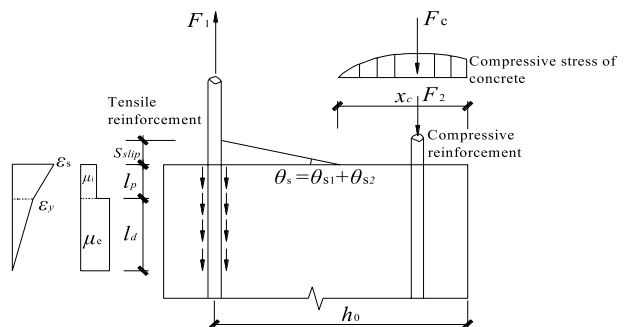
$$\gamma_y = \frac{f_{yh}}{E_s} + \frac{v_y - n}{\rho_v E_s} + \frac{4v_y}{E_c}, 0 \leq \frac{v_y - n}{\rho_v E_s} \leq \frac{f_{yh}}{E_s} \tag{28}$$

where μ_γ is the shear strain ductility coefficient; γ_y is the yield shear strain; γ_u is the ultimate shear strain; v_y is the yield shear stress; ρ_h is the ratio of stirrup reinforcement; ρ_v is the longitudinal reinforcement ratio; and f_{yv} is the stirrup yield strength.

(3) Lateral displacement caused by bond-slip Δ_{ms}

As shown in Fig. 12, the bond-slip between the longitudinal bars and concrete consists of the slip displacement generated in the upper elastic segment and the plastic hinge region. The rotation angle (θ_{s1}) of the rigid body due to bond-slip in the upper

Fig. 12 Bond strain and stress distribution for longitudinal bars



elastic segment can also be calculated by using the model proposed by Sezen-Setzler (2008). The rigid body rotation angle (θ_{s2}) due to the slip of longitudinal bars in the plastic hinge region is mainly related to the plastic hinge length and the strain in longitudinal bars. The bond strain and stress distribution for the longitudinal bars in the slip region are shown in Fig. 12. Δ_{ms} can be obtained from

$$\Delta_{ms} = (\theta_{s1} + \theta_{s2})l \tag{29}$$

where

$$\theta_{s1} = \frac{\epsilon_y f_y d_b}{8\mu_e (h_0 - x_c)} \tag{30}$$

$$\theta_{s2} = \frac{l_p (\epsilon_y + \epsilon_s)}{2(h_0 - x_c)} \tag{31}$$

3.5 Ultimate point

3.5.1 Ultimate force

The failure force is taken as 0.85 times the previous peak load (JGJ3-2010 2010): $P_u = 0.85P_m$ (32).

3.5.2 Ultimate displacement

When the failure is closed, the concrete in the plastic hinge area is seriously damaged, buckling of the longitudinal bars occurs, and the concrete out of the core area is crushed. The cross-section curvature distribution of the specimen at this point is shown in Fig. 12. The height of the plastic hinge area at the bottom of the specimen is still l_p , the outside plastic hinge area is still in the elastic stage, and the cross-section curvature of the plastic hinge area reaches the ultimate curvature. The lateral displacement of the specimen is mainly divided into the displacements generated by the upper elastic segment and the plastic hinge region. Among them, the displacements are all composed of the displacements generated by flexure, shear and reinforcing bar slip, as shown in Eq. (33).

$$\Delta_u = \Delta_{uf} + \Delta_{uv} + \Delta_{us} \tag{33}$$

where Δ_{uf} , Δ_{uv} and Δ_{us} are the flexure, shear and bond slip displacements at the ultimate point, respectively.

(1) Flexure displacement Δ_{uf} .

The flexure displacement is composed of the displacement Δ_{uf1} of the upper elastic segment and the displacement Δ_{uf2} of the plastic hinge region. $\Delta_{uf} = \Delta_{uf1} + \Delta_{uf2}$. The displacement Δ_{uf1} can be calculated by Eqs. (10–11). The displacement Δ_{uf2} can be obtained from

$$\Delta_{uf2} = \int_{l_e}^{l_e+l_p} \phi(u)xdx = \frac{1}{2}\phi(u)l_p^2 + \phi(u)l_e l_p \tag{34}$$

(2) Shear displacement Δ_{uv} .

The ultimate displacement caused by shear is composed of displacement Δ_{uv1} of the upper elastic section and displacement Δ_{uv2} of the plastic hinge region: $\Delta_{mv} = \Delta_{uv1} + \Delta_{uv2}$. The displacement Δ_{uv1} can be calculated from Eq. (12), and the column height l in the equation is replaced by the upper elastic section height l_e . The shear force V is replaced by the ultimate load. Δ_{mv2} can be obtained from the shear strain ductility coefficient μ_γ proposed by Gerin-Adebar (2004). The displacement Δ_{uv2} can be expressed as follows:

$$\Delta_{uv2} = \gamma_u l_p = \mu_\gamma \gamma_y l_p = \left(4 - 12 \frac{v_y}{f_c}\right) \gamma_y l_p \tag{35}$$

(3) Lateral displacement caused by bond-slip Δ_{us} .

The rotation angle (θ_{s1}) of the rigid body due to bond-slip in the upper elastic segment can also be calculated by the method proposed by Sezen-Setzler (2008). The displacement due to bond slip can be obtained from

$$\Delta_{us} = (\theta_{s1} + \theta_{s2})l \tag{36}$$

where

$$\theta_{s2} = \frac{l_p(\epsilon_y + \epsilon_s)}{2(h_0 - x_c)} \tag{37}$$

where ϵ_s is the strain when the tensile longitudinal reinforcement reaches the ultimate tensile strength. According to previous low-cycle reciprocating fatigue performance tests for high-strength reinforcement (Li et al. 2005), ϵ_s is taken to be equal to 0.035.

4 Discussion

4.1 Prediction of the characteristic points

Table 3 summarizes a comparison of the analytical and experimental values obtained for the yield force for the above four column specimens. The mean value for the analytical to experimental yield force ratio is 1.0, and the coefficient of variation is 0.06, so it can be seen that the proposed model can well predict the yield force for concrete columns built with HRB600 steel bars.

Table 4 lists the analytical and experimental values for the yield displacements of the above column specimens. The mean value for the analytical to experimental yield displacement ratio is 1.03, and the coefficient of variation is 0.11, so it can be seen that the proposed method has reasonable accuracy. The yield displacement is mainly caused by the bending moment, and the shear displacement is very small and can be ignored.

Table 5 lists the analytical and experimental values for the peak load of the above four column specimens. The height values for the equivalent rectangular stress diagrams of specimens HH-0.2–3, HH-0.2–4 and HH-0.4–5 are 90.7 mm, 90.7 mm and 121.1 mm,

Table 3 Analytical and experimental values for the yield force

Specimens	Loading direction	l/mm	$M_y/kN\cdot m$	Analytical $P_{y,c}/kN$	Experimental $P_{y,t}/kN$	$P_{y,c}/P_{y,t}$
NN-0.2-1	+	1123	192.0	171.0	156.9	1.09
	−	1123	192.0	171.0	158.9	1.08
NH-0.2-2	+	1095	192.0	175.3	164.8	1.06
	−	1095	192.0	175.3	164.7	1.06
HH-0.2-3	+	1115	228.3	204.8	202.1	1.01
	−	1115	228.3	204.8	205.7	1.00
HH-0.2-4	+	1080	228.3	211.4	209.7	1.01
	−	1080	228.3	211.4	206.7	1.02
HH-0.4-5	+	1090	275.0	252.3	268.2	0.94
	−	1090	275.0	252.3	266.8	0.95
HH-0.5-6	+	1090	294.4	270.1	301.3	0.90
	−	1090	294.4	270.1	302.1	0.89

l is the shear span of the column; $P_{y,c}$ and $P_{y,t}$ are the analytical and experimental yield forces, respectively

Table 4 Analytical and experimental values for the yield displacement

Specimens	ϕ_y/m^{-1}	$\Delta_{y,t}/mm$	$\Delta_{y,v}/mm$	$\Delta_{y,s}/mm$	$\Delta_{y,c}/mm$	$\Delta_{y,t}/mm$	$\Delta_{y,c}/\Delta_{y,t}$
NN-0.2-1	0.0108	5.36	0.14	2.43	7.93	8.19	0.97
NH-0.2-2	0.0108	5.10	0.14	2.37	7.61	7.06	1.08
HH-0.2-3	0.0160	6.81	0.16	4.07	11.04	11.32	0.98
HH-0.2-4	0.0160	6.39	0.16	3.94	10.49	11.77	0.89
HH-0.4-5	0.0186	7.67	0.20	4.69	12.55	12.08	1.04
HH-0.5-6	0.0204	8.34	0.21	5.10	13.65	11.00	1.24

$\Delta_{y,c}$ and $\Delta_{y,t}$ are the analytical and experimental yield displacements, respectively

respectively, which are all less than $\xi_b h_0$. For specimen HH-0.5–6, due to the larger axial load, $x=135.2$ mm, which is greater than $\xi_b h_0=130.1$ mm, the specimen suffers a small eccentric compression failure, which is consistent with the test results. M_u can be calculated according to Eq. (15), and then the peak load P_m can be obtained from $P_m = M_u / (l - \nu h)$. ν is the influence of the upward movement of the plastic hinge position due to the restriction of the foundation beam on the column bottom. ν is considered to range between 0.2 and 0.5, and a value of $\nu=0.3$ is adopted in this paper. The mean value for the analytical to experimental peak force ratio is 0.88, and the coefficient of variation is 0.08, so it can be seen that the proposed method can well predict the peak force for the columns.

The displacements (Δ_{mf} , Δ_{mv} , Δ_{ms}) at the peak point can be obtained from the above equations. Table 6 lists the analytical and experimental values for the peak displacements of the above column specimens. The mean value for the analytical to experimental peak displacement ratio is 0.99, and the coefficient of variation is 0.06, so it can be seen that the proposed method has a reasonable prediction accuracy.

Table 7 lists the analytical and experimental values for the ultimate displacement, and the proportion of the displacement caused by the bond-slip is the largest. The mean value

Table 5 Comparison of the analytical and experimental values obtained for the peak force

Specimen	Loading direction	x/mm	$M_u/kN\cdot m$	$P_{m,c}/kN$	$P_{m,t}/kN$	$P_{m,c}/P_{m,t}$
NN-0.2-1	+	80.2	223.1	219.2	237.8	0.92
	–	80.2	223.1	219.2	226.6	0.97
NH-0.2-2	+	80.2	223.1	225.4	262.0	0.86
	–	80.2	223.1	225.4	273.0	0.83
HH-0.2-3	+	90.7	257.0	254.5	285.8	0.89
	–	90.7	257.0	254.5	287.9	0.88
HH-0.2-4	+	90.7	257.0	263.6	292.8	0.90
	–	90.7	257.0	263.6	287.9	0.92
HH-0.4-5	+	121.1	283.0	287.3	308.9	0.93
	–	121.1	283.0	287.3	363.2	0.79
HH-0.5-6	+	136.0	294.4	298.9	406.2	0.74
	–	136.0	294.4	298.9	312.1	0.96

$P_{m,c}$ and $P_{m,t}$ are the analytical and experimental yield forces, respectively

Table 6 Analytical and experimental values for the peak displacement

Specimen	Δ_{mf1}/mm	Δ_{mf2}/mm	Δ_{mf}/mm	Δ_{mv1}/mm	Δ_{mv2}/mm	Δ_{mv}/mm	Δ_{ms}/mm	Δ_{mc}/mm	Δ_{mt}/mm	Δ_{mc}/Δ_{mt}
NN-0.2-1	3.69	5.92	9.61	0.14	1.12	1.26	8.39	19.26	19.81	0.97
NH-0.2-2	3.58	5.71	9.29	0.16	1.36	1.52	8.13	18.94	19.89	0.95
HH-0.2-3	4.44	6.80	11.23	0.17	1.79	1.96	11.33	24.52	25.01	0.98
HH-0.2-4	4.26	6.50	10.76	0.16	1.63	1.79	10.91	23.46	24.80	0.95
HH-0.4-5	5.07	5.88	10.96	0.19	1.45	1.64	11.27	23.86	24.71	0.97
HH-0.5-6	5.52	6.00	11.52	0.20	1.45	1.65	12.07	25.24	22.31	1.13

Δ_{mt} is the experimental yield displacement, which is taken as the average value of the positive and negative yield displacements

for the analytical to experimental ultimate displacement ratio is 0.92, and the coefficient of variation is 0.17. Due to the large axial compression ratio of HH-0.5–6, the P- Δ effect is obvious, which leads to a reduction in the deformation capacity and a small ultimate displacement in the specimens.

4.2 Predicted hysteretic curves

The above simplified method and finite element modeling are used to model the mechanical behavior of HRB600 bar reinforced concrete column specimens under cyclic loading, and the obtained analytical results are compared with the test results. OpenSees was used to model the hysteretic behavior of HRB600 bar reinforced concrete columns. To accurately simulate the hysteretic performance of the columns built with HRB600 reinforcement, the fibers of the cross-section are divided into reinforcement bars and concrete fibers

Table 7 The analytical and experimental values for ultimate displacement

Specimen	Δ_{ur1}/mm	Δ_{ur2}/mm	Δ_{ur}/mm	Δ_{uv1}/mm	Δ_{uv2}/mm	Δ_{uv}/mm	Δ_{uc}/mm	Δ_{uc}/mm	Δ_{ut}/mm	Δ_{uc}/Δ_{ut}
NN-0.2-1	3.69	8.37	12.06	0.12	1.50	1.63	33.75	47.43	56.62	0.84
NH-0.2-2	3.58	8.07	11.65	0.14	1.61	1.74	32.64	46.04	59.8	0.77
HH-0.2-3	4.44	8.32	12.75	0.14	2.43	2.57	36.56	51.88	51.75	1.00
HH-0.2-4	4.26	7.95	12.21	0.14	1.92	2.06	35.12	49.39	60.95	0.81
HH-0.4-5	5.07	6.83	11.90	0.16	1.71	1.87	39.74	53.51	62.02	0.86
HH-0.5-6	5.52	6.00	11.52	0.17	1.71	1.88	41.99	55.39	45.25	1.22

Δ_{ur} is the experimental ultimate displacement, which is taken as the average value of the positive and negative ultimate displacements

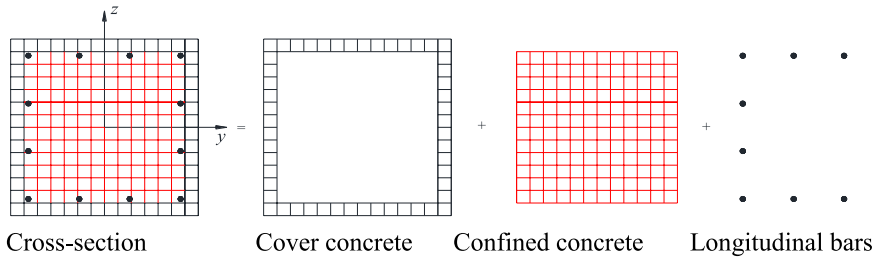


Fig. 13 Fiber element arrangement of the finite model (OpenSees)

depending on the material types, as shown in Fig. 13. According to the different confinement conditions of concrete at the cross-section, concrete fibers can be divided into two areas: concrete fibers in the cover area and confinement concrete fibers in the core area. Figure 14 presents a comparison of the analytical, simulated, and experimental hysteretic curves obtained for the HRB600 longitudinal bar reinforced concrete column specimen. To evaluate the accuracy of the predicted hysteretic curves, the analytical skeleton curves and energy dissipation were compared with the simulated and experimental curves. Figure 15 presents a comparison of the skeleton curves obtained using the analytical, simulated, and experimental hysteretic curves shown in Fig. 14. The error range for the predicted to experimental strength is 4%~26%, and the error range for the predicted to experimental deformation capacity is 0~19%. Therefore, the proposed model can be used to well predict the strength and deformation of HRB600 longitudinal bar reinforced concrete columns. The energy dissipation capacity is an important index for the seismic performance of RC members. (Fig. 15) The energy dissipated by the members is indicated by the area surrounded by the hysteresis loops. Figure 16 shows a comparison of the variation in the experimental, simulated and analytical dissipated energy with increasing lateral displacement. The maximum error in the predicted to experimental dissipated energy is 20%, with both values showing a reasonable agreement.

In conclusion, the analytical and simulated hysteresis curves are in reasonable agreement with the experimental hysteretic curves in terms of energy dissipation, strength, and deformation capacity, indicating that the proposed hysteretic model can be used to well predict the hysteresis performance of HS bar reinforced concrete columns under cyclic loading. It also shows that the proposed model can achieve a prediction accuracy similar to that of the finite element software OpenSees.

5 Conclusions

In this paper, cyclic tests were conducted to examine the effect of the reinforcement strength, axial load ratio and stirrup spacing on the seismic performance of concrete columns built with HRB600 reinforcement. A hysteretic model for HS bar reinforced columns is proposed, and its prediction accuracy is evaluated based on the test data. The following conclusions can be drawn:

- (1) The skeleton curve and hysteretic rule can be combined to establish a calculation model for concrete columns built with HS and normal strength reinforcement. The skeleton

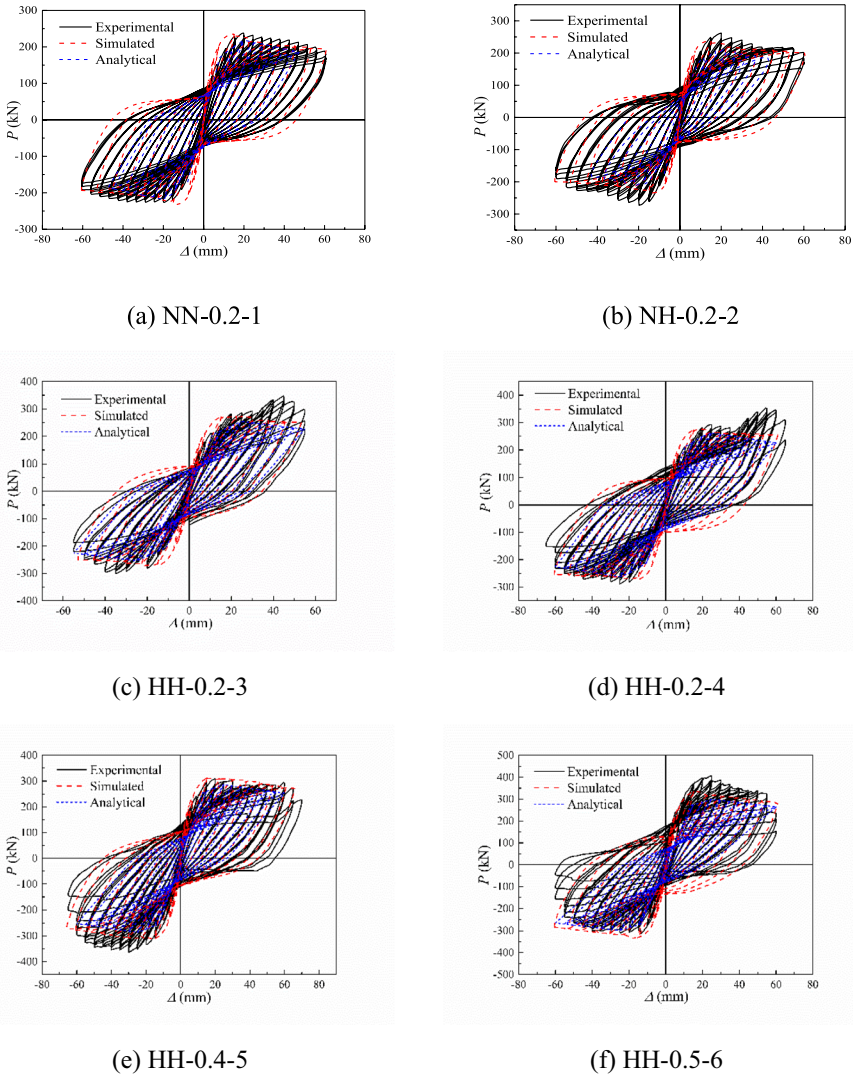


Fig. 14 Comparison of the hysteresis curves

curve is simplified as a trilinear model represented by yield, peak and ultimate points. By deriving the formulas for yield, peak and ultimate force and displacement, a method can be obtained for determining the skeleton curve. A hysteretic rule is established based on the experimental hysteretic curves shown in this paper.

- (2) The equations for the flexure strength are derived based on the theory of the Bernoulli–Euler assumption. The lateral deformation is assumed to be composed of flexure, shear, and bond-slip deformations. The equations for the flexure deformation are derived based on plastic hinge theory, the equations for shear deformation are derived based on elastic mechanics, and bond-slip deformations are calculated according to the actual contact stress between HS longitudinal bars and concrete. These studies demonstrate that the proposed equations have reasonable accuracy.

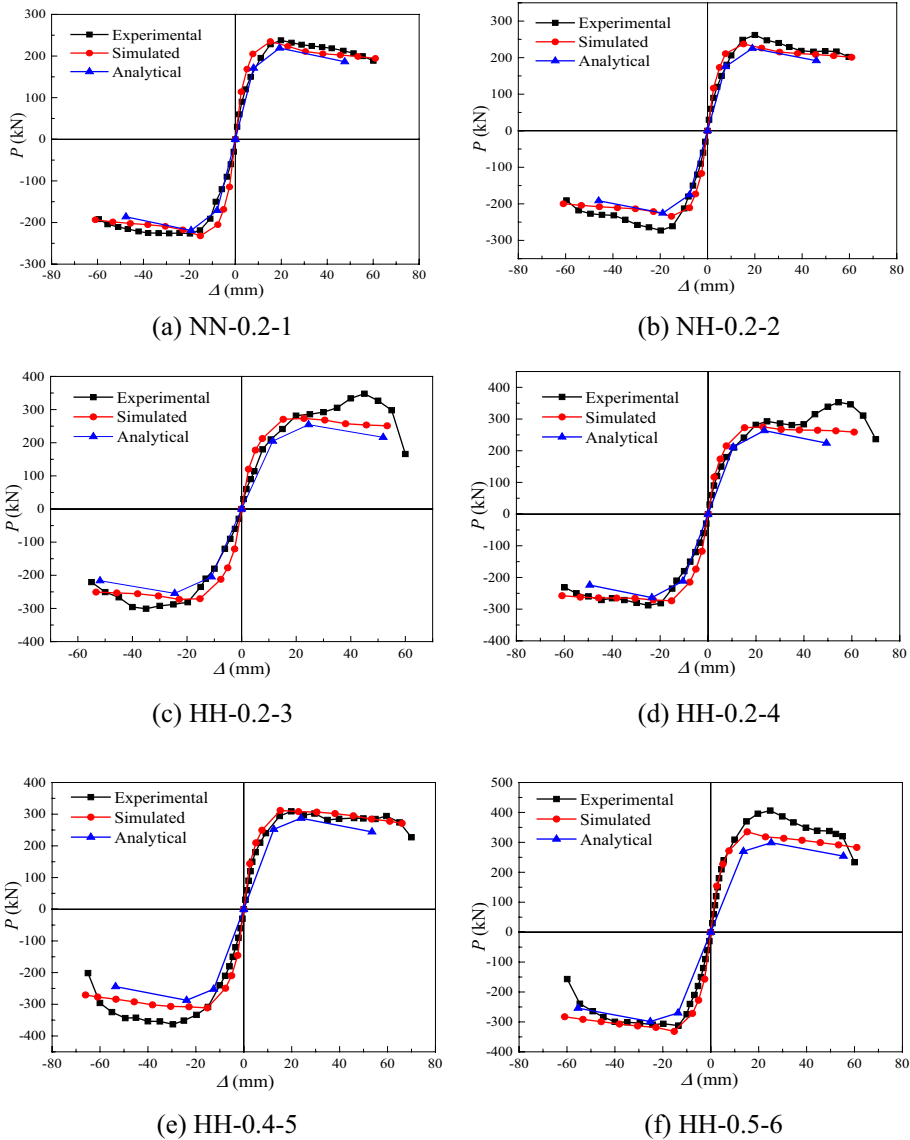


Fig. 15 Comparison for the skeleton curves

- (3) The proposed model is used to calculate the hysteretic curves for HS and normal-strength bar reinforced concrete columns, which are compared with the experimental curves. The research results show that the analytical hysteresis curves are in good agreement with the experimental hysteretic curves in terms of strength, deformation and energy dissipation.

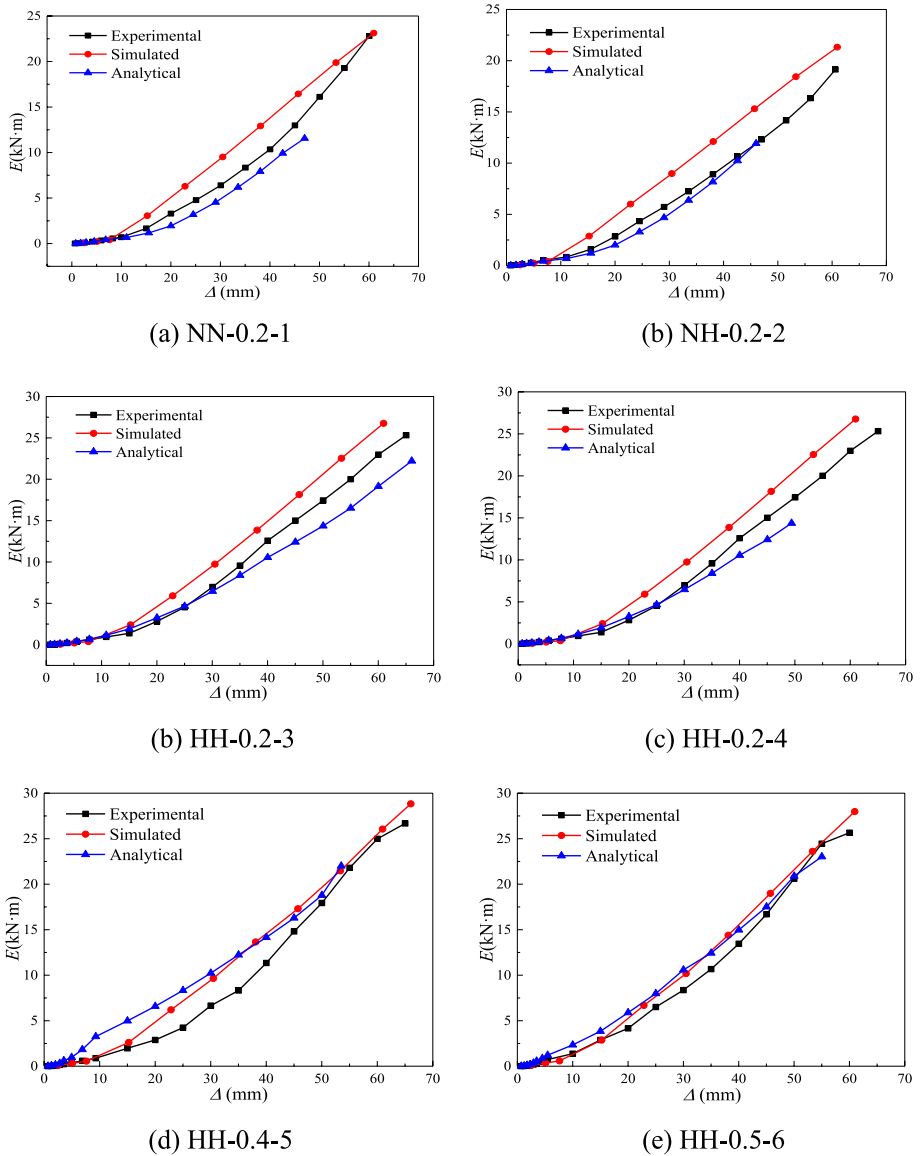


Fig. 16 Comparison for the energy dissipation

Funding The authors would like to acknowledge the support from the National Postdoctoral Program for Innovative Talents (Grant No.: BX20200246) and the Open Project of the Key Laboratory of Concrete and Prestressed Concrete Structures of the Ministry of Education, Southeast University (Grant No.: CPCSM2022-05).

Data availability statement The data that support the findings of this study are available on request from the corresponding author. The data are not publicly available due to privacy or ethical restrictions.

Declarations

Conflict of interest The authors proclaim that they have no known contending monetary interests or individual connections that might have seemed to impact the work announced in this paper.

References

- Aboukifa M, Moustafa MA (2021) Experimental seismic behavior of ultra-high performance concrete columns with high strength steel reinforcement. *Eng Struct* 232:111885
- Ding Y, Wu D, Su J, Li ZX, Zong L (2021) Feng K (2021) Experimental and numerical investigations on seismic performance of RC bridge piers considering buckling and low-cycle fatigue of high strength steel bars. *Eng Struct* 227:111464
- GB 50010–2010. 2011. Code for design of concrete structures. China Architecture 625 & Building Press, Beijing, China. (in Chinese)
- Gerin M, Adebar P (2004) Accounting for shear in seismic analysis of concrete structures. 13th world conference on earthquake engineering, Vancouver, Canada.
- Guo ZX, Xilin Lu (2004) Experimental study on the hysteretic model of rc columns with high axial compressive ratio. *Chin Civil Eng J* 37(5):32–38
- He S, Deng Z, Yao J (2020) Seismic behavior of ultra-high performance concrete long columns reinforced with high-strength steel. *J Build Eng* 32:101740
- Hwang SK, Yun HD, Park WS, Han BC (2005) Seismic performance of high-strength concrete columns. *Mag Concr Res* 57(5):247–260
- Hwang H-J, Park H-G, Choi W-S, Chung L, Kim Jin-Keun (2014) Cyclic Loading test for beam-column connections with 600 MPa (87 ksi) Beam flexural reinforcing bars. *ACI Struct J*. <https://doi.org/10.14359/51686920>
- Ibarra L, Bishaw B (2016) High-strength fiber-reinforced concrete beam-columns with high-strength steel. *ACI Struct J* 113(1):147–156
- JGJ3–2010. 2010. Technical specification for concrete structures of tall building. Beijing: China Construction Press. (in Chinese)
- Lepage A, Tavallali H, Pujol S, Rautenberg JM (2012) High-performance steel bars and fibers as concrete reinforcement for seismic-resistant frames. *Adv in Civil Engineering* 2012:1–13
- Li Y, Cao S, Jing D (2018) Concrete columns reinforced with high-strength steel subjected to reversed cycle loading. *ACI Struct J*. <https://doi.org/10.14359/51701296>
- Li J (2005) Study on the performance of steel reinforced high-strength concrete columns under low cyclic reversed loading. Dissertation, Xi'an University of Architecture and Technology, Xi'an, China
- Li Y, Aoude H (2019) Blast response of beams built with high-strength concrete and high-strength ASTM A1035 bars. *Int J Impact Eng* 130:41–67
- Li S, Zicheng Z (2014) Study on restoring force model for high strength concrete columns confined by butt-welded closed composite high strength stirrups with high axial compression ratios. *Earthq Eng Eng Dynam* 34(6):188–197
- Lim JJ, Park HG, Eom TS (2017) Cyclic load tests of reinforced concrete columns with high-strength bundled bars. *ACI Struct J* 114(1):197–207
- Link T B (2014) Seismic performance of reinforcement concrete bridge columns constructed with grade 80 reinforcement. Master's thesis, Oregon State University, Corvallis, Oregon.
- Matsumoto T, Nishihara H, Nakao M (2008) Flexural performance on RC and precast concrete columns with ultra high strength materials under varying axial load. In: The 14th World Conference on Earthquake Engineering, Beijing, China, October 12–17 2008, p 138
- NEHRP Consultants Joint Venture (2014) Use of high-strength reinforcement in earthquake-resistant concrete structures. Technical report NIST GCR 14–917–30, National institute of standards and technology, Gaithersburg, Maryland
- Ni X, Cao S, Liang S, Li Y, Liu Y (2019) High-strength bar reinforced concrete walls: cyclic loading test and strength prediction. *Eng Struct* 198:109508
- Ou YC, Alrasyid H, Haber ZB, Lee HJ (2015) Cyclic behavior of precast high-strength reinforced concrete columns. *ACI Struct J* 112(6):839–850
- Ousalem H, Takatsu H, Ishikawa Y, Kimura H (2009) Use of high-strength bars for the seismic performance of high-strength concrete columns. *J Adv Concr Technol* 7(1):123–134
- Paultre P, Légeron F, Mongeau D (2001) Influence of concrete strength and transverse reinforcement yield strength on behavior of high-strength concrete columns. *ACI Struct J* 98(4):490–501

- Restrepo JI, Seible F, Stephan B, Schoettler MJ (2006) Seismic testing of bridge columns incorporating high-performance materials. *ACI Struct J* 103(4):496–504
- Rautenberg JM (2011) Drift capacity of concrete columns reinforced with high-strength steel. Dissertation, Purdue University
- Sezen H, Setzler EJ (2008) Reinforcement slip in reinforced concrete columns. *ACI Struct J* 105(3):280–289
- Shi QX, Kun Y, Ligeng B, Xinghu Z, Weishan J (2011) Experiments on seismic behavior of high-strength concrete columns confined with high-strength stirrups. *Chin Civil Eng J* 44(12):9–17
- Sokoli D (2014) Seismic performance of concrete columns reinforced with high-strength steel. The University of Texas at Austin, Texas
- Su J, Wang J, Wang W, Dong Z, Liu B (2014a) Comparative experimental research on seismic performance of rectangular concrete columns reinforced with high strength steel. *J Build Eng Struct* 11(35):20–27
- Su J, Wang J, Wang W, Mei S (2014b) Experimental study on seismic performance of circular columns confined by high-strength spiral stirrups. *Earthquake Engineering and Engineering Dynamics* 34(4):206–211
- Trejo D, Link TB, Barbosa AR (2016) Effect of reinforcement grade and ratio on seismic performance of reinforced concrete columns. *ACI Struct J* 113(5):907–916
- Thomsen JH, Wallace JW (1994) Lateral load behavior of reinforced concrete columns constructed using high-strength materials. *ACI Struct J* 91(5):605–615
- Thomsen IJH, Wallace JW (2004) Displacement-based design of slender reinforced concrete structural walls-experimental verification. *J Struct Eng ASCE* 130(4):618–630
- Wang Z, Wang JQ, Zhu JZ, Zhang J (2019a) A simplified method to assess seismic behavior of reinforced concrete columns. *Struct Concr* 21(1):151–168
- Wang Z, Wang J, Tang Y, Gao Y, Zhang J (2019b) Lateral behavior of precast segmental UHPC bridge columns based on the equivalent plastic-hinge model. *J Bridg Eng* 24(3):04018124
- Xiao Y, Martirosyan A (1998) Seismic performance of high-strength concrete columns. *J Struct Eng* 124(3):241–251
- Zhang J, Cai R, Li C, Liu X (2020) Seismic behavior of high-strength concrete columns reinforced with high-strength steel bars. *Eng Struct* 218:1108

Publisher's Note Springer Nature remains neutral with regard to jurisdictional claims in published maps and institutional affiliations.

Springer Nature or its licensor (e.g. a society or other partner) holds exclusive rights to this article under a publishing agreement with the author(s) or other rightsholder(s); author self-archiving of the accepted manuscript version of this article is solely governed by the terms of such publishing agreement and applicable law.